catalysts

MDPI

Article

The Role of Nanoparticle Catalysis in the Nylon Production

Lucia Tonucci [1,*], Andrea Mascitti [2], Anna M. Ferretti [3], Francesca Coccia [1] and Nicola d'Alessandro [2]

[1] Department of Philosophical, Educational and Economic Sciences, "G. d'Annunzio" University of Chieti-Pescara, 66100 Chieti, Italy
[2] Department of Engineering and Geology, "G. d'Annunzio" University of Chieti-Pescara, 65127 Pescara, Italy
[3] Istituto di Scienze e Tecnologie Chimiche "Giulio Natta" (SCITEC)—CNR, Laboratorio di Nanotecnologie, Sezione via G. Fantoli 16/15, 20138 Milano, Italy
* Correspondence: lucia.tonucci@unich.it; Tel.: +39-08713555340

Abstract: Renewal in the world production of plastics with growing amounts of building blocks from biomass is a pressing demand among society. Adipic acid is one of the monomers of nylon 6,6, and, traditionally, is obtained from fossil sources, but it is possible to reduce the muconic acids, deriving it from biomass, to obtain adipic acid. However, these catalyzed reactions use commonly hazardous conditions or reagents; in this study, a pathway to obtain a bio-adipic acid, following the Green Chemistry, is reported. Metal nanoparticles (M NPs; M = Pd, Pt, Ru, Rh) were synthesized in water at 80 °C using sodium lignosulphonate as a reducing and stabilizing agent. They were characterized by TEM and XRD techniques: Pd NPs were larger (21 nm) and spherical in shape; Pt NPs were irregular; Ru and Rh NPs were smallest (1.9 and 5.3 nm, respectively). M NPs were tested as catalyst in the hydrogenation reactions of dicarboxylic acids (fumaric, malonic, *trans*,*trans*- and *cis*,*cis*-muconic acids) in water at room pressure and temperature. The NPs transformed selectively fumaric and malonic acids to succinic acid, although with different yields. Ru and Pt NPs were moderately active while with Pd NPs, 80% of succinic acid was obtained and with Rh NPs, 100% was observed. Carrying out the hydrogenations on muconic acids at pH 5, the formation of adipic acid was observed with all NPs but selectivities in the presence of Ru, Pt and Pd NPs were not excellent. The selectivity with Rh NPs was remarkable (86% from *cis*,*cis*- and about 100% from *trans*,*trans*-muconic acid) considering the mild conditions; furthermore, it is attractive that the adipic acid was obtained also from the *cis*,*cis* isomer which can be produced from biomass.

Keywords: Lignin; adipic acid; metal nanoparticles; rhodium; reducing reaction; muconic acid; maleic acid; fumaric acid

Citation: Tonucci, L.; Mascitti, A.; Ferretti, A.M.; Coccia, F.; d'Alessandro, N. The role of Nanoparticle Catalysis in the Nylon Production. *Catalysts* **2022**, *12*, 1206. https://doi.org/10.3390/catal12101206

Academic Editor: Francesco Mauriello

Received: 13 September 2022
Accepted: 5 October 2022
Published: 10 October 2022

1. Introduction

Nylon is a dominating polymer in industrial applications: the global market size was estimated at $31.1 billion in 2021 and is expected to reach an annual growth of 6.2% by 2030 [1]. The replacement of traditional plastic (e.g., PVC) in sectors like automotive and electronics, with the engineered ones will push up the nylon 6,6 market growth [2]: consumption of nylon (6 and 6,6) is expected to reach 2.8 million tons by 2025 in Europe alone [3].

The reagents to obtain nylon 6,6 are adipic acid (hexanedioic acid) and hexamethylenediamine; the traditional production of adipic acid starts from petroleum-derived cyclohexane transformation to cyclohexanol and cyclohexanone mixture oxidized by nitric acid [4]. Unfortunately, this process releases N_2O in high amounts (about 0.3 ton per ton of adipic acid) promoting, in this way, global warming [5,6] even if it can be recovered as nitric acid at the end of the process [7]. Furthermore, the use of fossil sources and toxic or hazardous reagents and solvents is not desirable according to the Green Chemistry principles [8]. Considering the large polymers market, a slight decrease of fossil or toxic

feedstock can be of great progress for the innovative bio-industry and a formidable benefit for the environment.

In recent years, several alternative syntheses of adipic acid were published [9–13], but a huge green step will be achieved using directly muconic acid (hexa-2,4-dienedioic acid), from biomass, as a starting compound. Adipic acid is a drop-in chemical because, when biobased, it could replace the fossil one without altering the subsequent industrial productive chain; the high number of patents, furthermore, makes it a business-driven compound [14]. The muconic acid can be employed mostly as *cis,cis*- or *trans,trans*-isomer. The isomer *cis,cis* of muconic acid ((2*Z*,4*Z*)-hexa-2,4-dienedioic acid) can be obtained from biomass, by the biotransformation of aromatics [15,16], de novo synthesis of glucose [17,18] or from lignin [19–21] with engineered *Pseudomonas putida*, although the catalytic hydrogenation of *trans,trans*-muconic acid ((2*E*,4*E*)-hexa-2,4-dienedioic acid) to adipic acid was more reported in literature due to the high stability of this isomer, which simplifies the kinetic study of the reaction excluding potential isomerization steps [22]. Several works showed that *trans,trans*-muconic acid can be produced via chemical isomerization of biobased *cis,cis*-muconic [23–25] and then the formation of adipic acid could be achieved by two steps, and also in one-pot: the *cis,cis*-muconic acid isomerization to *trans,trans* and the successive hydrogenation to adipic acid. Between the recently published hydrogenations of *trans,trans*-muconic, we can cite the reaction with Re/TiO_2 in methanol at 210 °C and 69 bar of hydrogen [26], with Pt/C in water at 7 bar of hydrogen and room temperature [27], in the presence of Pd/C at 50°–70 °C and 1 bar of hydrogen [28,29]. The isomerization of *cis,cis*-muconic acid, however, is not always a quantitative reaction because of the formation of intramolecular lactonized forms of muconic acid [23]. The direct chemical transformation of *cis,cis*-muconic (or its ester form) to adipic acid, by selective hydrogenation, recently, was achieved in several reaction conditions: using Pd/C or Rh/C as catalyst at 24 °C and 24 bar of hydrogen in ethanol solution [20,30]; in water with Ni/alumina at 60 °C and 10 bar of hydrogen [31]; in methanol at 175 °C with Re/C in absence of external hydrogen but in an inert atmosphere [32].

The scientific community is excited by the potential use of *cis,cis*-muconic acid as industrial platform, but, in our opinion, the reaction conditions can be improved in terms of sustainability, reducing the temperature and/or hydrogen pressure, selecting an appropriate solvent and a metal catalyst greener, less expensive and not hazardous. So, to sum, combining a biotechnological step for the fermentative production of the bio-based *cis,cis*-muconic acid with its catalytic conversion to adipic acid could be a novel pathway to start greening the production of nylon. In addition, the other reagent, the hexamethylenediamine, can be biomass-derived: hydroxymethylfurfural, in the "Top 10" list of the biobased chemicals [33], is a potential product of photooxidation of the lignin [34] and can be transformed in hexamethylenediamine [35].

Lignin is an underutilized waste-biomass, often used as a source of thermal energy, but essential in a sustainable industry transformation [16]; its aromatic polymer nature makes it a resource for chemicals and building blocks [34,36–39], innovative products [25,40,41], and alternative fuels [42,43]. Lignin valorization is key for the future development of the green industry. Recently, we prepared several Pt and Pd nanoparticles (Pd NPs and Pt NPs), stabilized with lignin [44], and used as catalysts at mild conditions in the cross-coupling [45], hydrogenation [46], and reduction reactions [47].

In this work, we presented our Pd and Pt nanoparticles, new Ru and Rh ones (Ru NPs and Rh NPs), still stabilized by lignin [44]. Rh and Ru have been selected between the platinum group metals for their catalytic activity *versus* C-H bond and in the selective reduction of C=C in styrene [48], benzene [49,50], aromatics [51], cyclohexene and its derivatives [52], butadiene [53], eugenol [54].

All M NPs were characterized by TEM, XRD and UV-vis and tested as catalysts in the selective hydrogenation, in mild conditions, of α,β-unsaturated dicarboxylic acid models, i.e., fumaric acid ((2*E*)-but-2-enedioic acid) and maleic acid ((2*Z*)-but-2-enedioic acid) to corresponding succinic acid (butanedioic acid), evaluating their activity and

selectivity. Furthermore, the catalytic system was tested on *trans,trans*- and *cis,cis*-muconic acid to obtain the adipic acid.

In this way, we can suggest an important role for the lignin in a potential future production of nylon 6,6, following the Scheme 1.

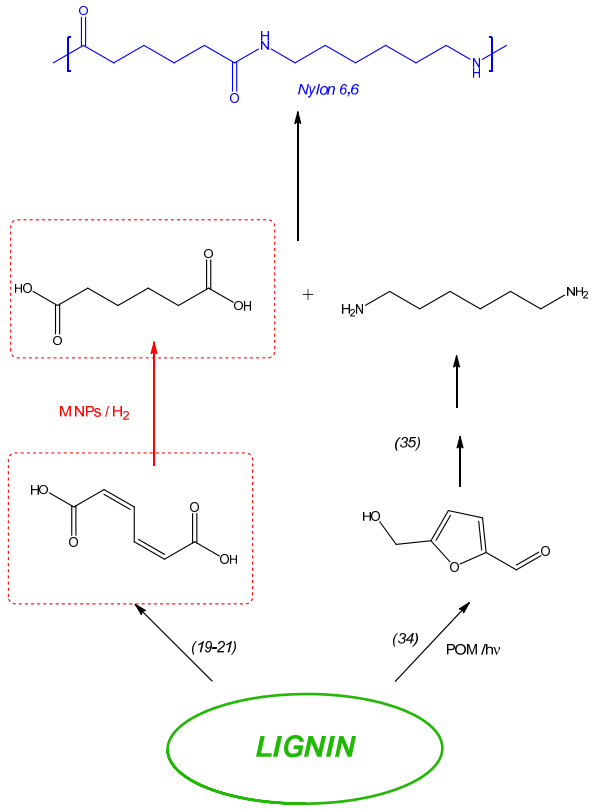

Scheme 1. The suggested pathway for a green production of nylon 6,6 from lignin. In black, the transformations in literature, in red our proposed preparation of adipic acid.

2. Results and Discussion

We synthesized four types of M NPs using Pt, Pd, Ru or Rh salts and the sodium lignosulphonate (NaLig); briefly, at 80 °C in water solution, the lignin acted as reducing agent for metal ions (i.e., Pt^{2+}, Pd^{2+}, Ru^{3+}, Rh^{3+}) and stabilizing the NPs simultaneously [44]. The formation of NPs was signalled by the solutions which got darker in colour (from brown to black and to dark brown in the case of Pd and Ru; from orange to light brown for Rh and to dark brown for Pt, without solid precipitates).

The studied NPs were deeply characterized by TEM. These M NPs showed different size and dispersion in dimension. The Pd NPs had largest mean diameter (d_m) and were extremely dispersed in size (d_m = 21.6 ± 9.2 nm and a dispersion of 42.6%). The Pd NPs were reported in Figure 1a,b: the lignin around the NPs is well visible, the thickness of the lignin shell is not constant. The percentage of active atoms on the surface is 56.7% ± 0.6 [55]. The Pt NPs were smaller and irregular with strong tendency to aggregate (Figure S1), as early reported [44]. The Rh NPs had smaller size; the shape is spherical, and the dispersion is sharp (d_m = 5.3 ± 1.5 nm and a dispersion is 28.3%). The NPs resulted in being uniformly distributed and surrounded by the lignin, as it was depicted in the reported image (Figure 1c,d). The NPs, in the TEM images, seemed to be deposited on a layer of lignin. The percentage of catalytically active atoms on the NPs is 59.1% ± 1.0 [55]. The Ru NPs were the smallest of the prepared samples (d_m = 1.9 ± 0.5 nm with a size dispersion of 26.3%). The NPs were supported and well distributed; they did not show any agglomerates and resulted in being deposited on a lignin layer (Figure 1e,f). The percentage of

catalytically active atoms on the NPs is 65.7% ± 3.2, which is the highest as expected: smaller is the NP, higher is the percentage of atoms on the surface of the NPs [55].

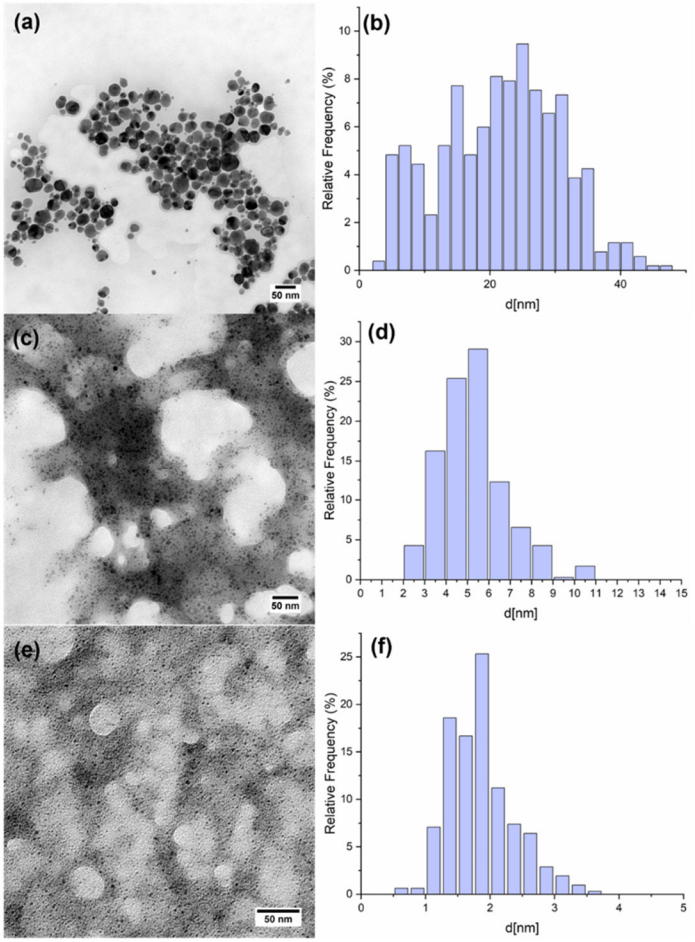

Figure 1. On the left: TEM images of (**a**) Pd NPs, (**c**) Rh NPs and (**e**) Ru NPs and the corresponding histogram distribution of the diameter on the right in the (**b**,**d**,**f**) panel.

The UV-vis spectra of Pd and Pt NPs were already published [44]; briefly, Pd NPs solution showed a weak plasmon absorption, in the visible region, derived from the formation of nanostructures, and Pt NPs showed only the disappearance of the signals attributable to Pt ions. The spectra of Ru and Rh NPs revealed a slight increase of absorbance in the visible region compared to the initial solutions of salt and lignin, attributable to the formation of NPs with very small size (Figures S2 and S3) [56,57].

In the XRD experiments, the formation of a crystalline phase, attributable to the presence of NPs with metals in the zero-valent state, was observed in the case of Pt and Pd NPs, as previously reported [44]. In the case of Rh (Figure S4), the broad signal attributable to the amorphous state of lignin was dominant (5°–35° 2θ, Figure S5) and it was very problematic to detect the peaks (e.g., around 42° and 48°) from Rh^0 [58], even if the disappearance of the $RhCl_3$ signals was easier to see (Figure S6). The apparent absence of the Rh^0 peaks was due to their extreme lowering typical of the dispersed NPs and with small size, as previously reported [59]. Ru NPs XRD looked similar (Figures S7 and S8) probably for the same reasons [60].

The NPs were stable for 30 days in air and at 20 °C.

In the presence of Pt, Pd, Ru and Rh NPs as catalysts, we performed the hydrogenation of α,β-unsaturated dicarboxylic acids, i.e., fumaric acid, maleic acid, *cis*,*cis*- and *trans*,*trans*-muconic acids (Scheme 2). The reactions conditions were green and mild: 20 mM of substrate in water, 100 mL of M NPs solution (corresponding to 0.037 mM of the

metal), room pressure of H_2, 20 °C, 8 h. The course of reaction, with conversion and yield, was evaluated by ^{1}H NMR spectra at pre-set time intervals (0, 1, 2, 4, 8 h). In the absence of M NPs, with lignin under hydrogen atmosphere or in air in the presence of the M NPS, no transformation of substrates was observed.

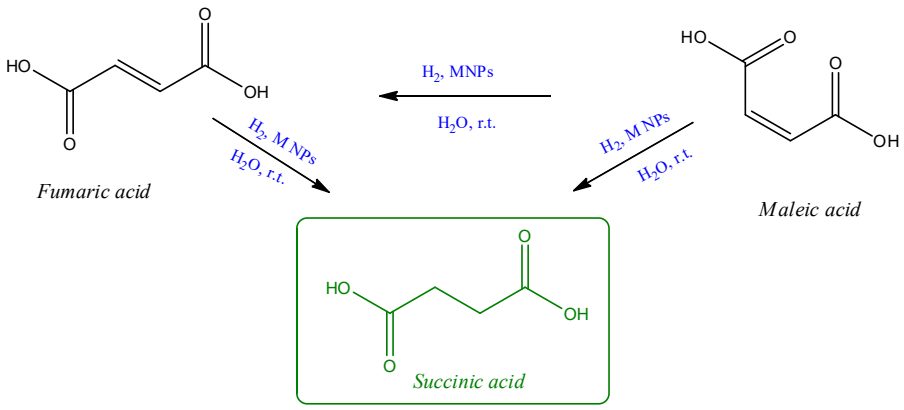

Scheme 2. The hydrogenation of 2-butenedioic acids to succinic acid, in presence of M NPs (M = Pd, Pt, Ru, Rh).

2-Butenedioic acids, as model compounds, were very informative and useful in tuning the reactions conditions to apply with the target compounds of this study. The conversions were always resulted superimposable to the yields of succinic acid for both isomers, making the selectivity of all metal NPs always 100% (Figures 2 and 3). In the hydrogenation of maleic acid, the yield in presence of Ru NPs was just sufficient (19% in 8 h, Figures 2, S17 and S18), with only subtle difference (<1%) in the last four hours of the reaction (Figure S9). The yields after 8 h in the presence of Pt and Pd NPs were very high, 60% and 77% respectively (Figures 2, S10 and S11); with Rh NPs we observed a quantitative transformation of maleic acid in succinic acid, already complete in 4 h (Figures 2, S12, S19 and S20). It is interesting to emphasize that, in the ^{1}H NMR spectra, the fumaric acid (at 6.72 ppm) was observed occasionally during the course of the hydrogenation only in amounts that were too low to be reliably measurable (< 2%).

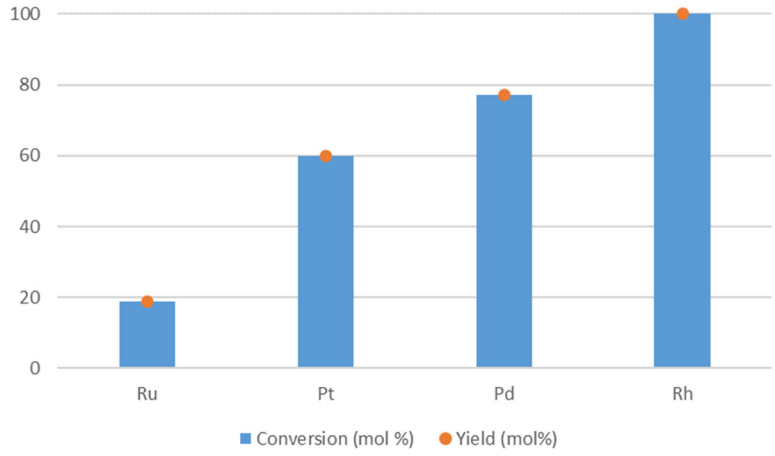

Figure 2. The conversion (mol%, blue) and yield (mol%, orange) of the hydrogenation reactions of maleic acid in presence of Ru, Pt, Pd and Rh NPs (metal = 0.037 mM) in water at room temperature and pressure with H_2 after 8 h of reaction.

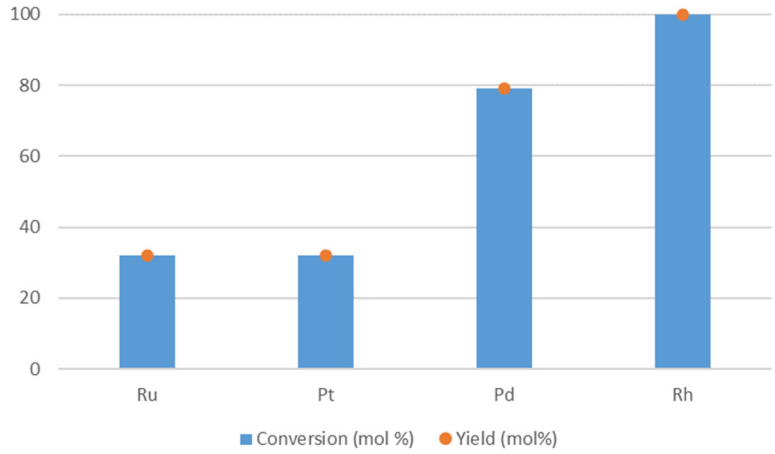

Figure 3. The conversion (mol%, blue) and yield (mol%, orange) of the hydrogenation reactions of fumaric acid in presence of Ru, Pt, Pd and Rh NPs (metal = 0.037 mM) in water at room temperature and pressure with H_2 after 8 h of reaction.

Also in the case of fumaric acid, the Ru and the Pt NPs were less active. In fact, the yields with Ru and Pt were both 32% at 8 h, against 79% in presence of Pd; Rh NPs was the most active catalyst converting 100% of the starting compound (Figures 3, S13–S16 and S21–S24).

From these results, Ru NPs was resulted as moderately active, even if highly selective, catalyst in the reduction of the model compound; Pd, Pt and Rh have proven to be very good catalysts.

The effect of increasing amounts of catalyst was studied with the metal that showed the best activity (Rh NPs) in the reduction of both 2-butenedioic acids. Tests were carried out with 10 μL (0.0037 mM in Rh), 50 μL (0.0185 mM), 300 μL (0.111 mM), 500 μL (0.185 mM) of Rh NPs solution, comparing the results with that above described, observed carrying out the hydrogenations with 100 μL (0.037 mM). With the lowest concentration of the metal, the conversions were not quantitative after 8 h under hydrogen; increasing the catalyst to 0.0185 mM, the conversions reached 100% only after 8 h, whereas with Rh 0.037 or 0.111 mM the conversions were quantitative even after 4 h (Table S1). In presence of the highest amount of metal (0.185 mM), the conversions were ranging from 60 to 80%; the selectivity with maleic acid decreased and the fumaric acid, as by-product, was observed also in the final NMR spectra. The selected concentration of metal (0.037 mM) was, in our opinion, the best choice, saving the metal and the time.

Therefore, we tested all NPs at 0.037 mM of metal for the hydrogenation reaction of muconic acids to obtain adipic acid. In order to promote the solubilization of the muconic acids, the pH of the water solution was adjusted at 5 with NaOH. Our NPs resulted in being less active for the reduction of more recalcitrant hexenedioic acids, particularly in the case of the *trans,trans* compound: the conversions of this unsaturated acid were ranging from 10% with Pt and Ru NPs to 25% with Rh NPs (after 8 h of the reaction, Figures 4 and S25–S28). The quantitative and qualitative results were obtained by ^{1}H NMR spectra of the reaction mixture (Figures S38–S42). The adipic acid was the predominant product: its yields were about 2%, 7%, 13% and 25% in presence of Ru, Pt, Pd and Rh, respectively. The other products were the isomers of monounsaturated hexendioic acid, namely 3-hexenedioic acid and 2-hexenedioic acid (Scheme 3); no lactone formation or decarboxylated products were observed. The most abundant monounsaturated was 2-hexenedioic acid; instead, 3-hexenedioic acid did not exceed 2% yield (Table S2).

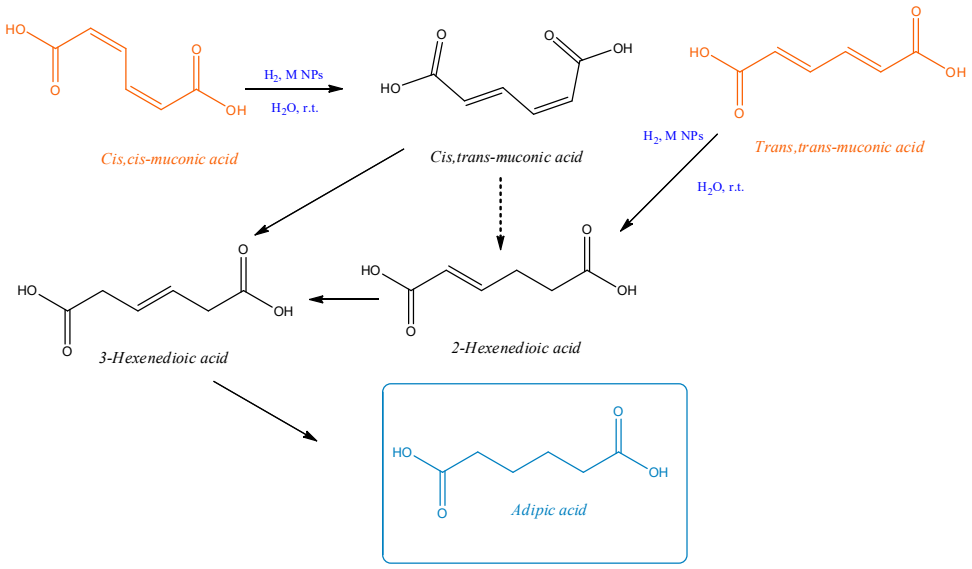

Scheme 3. The hydrogenation of muconic acids to adipic acid, in presence of M NPs (M = Pd, Pt, Ru, Rh).

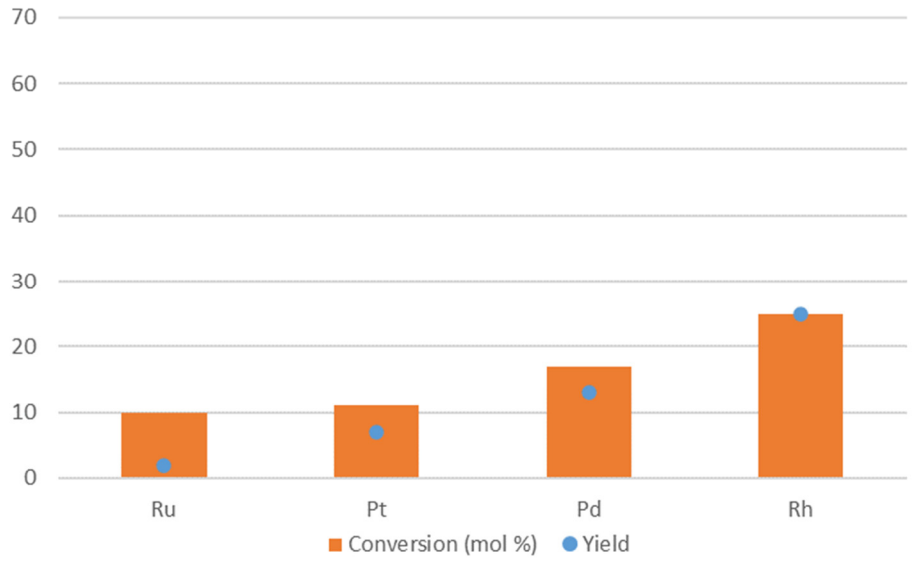

Figure 4. The conversion (mol%, orange) and yield (mol%, blue) of the hydrogenation reactions of *trans,trans*-muconic acid in presence of Ru, Pt, Pd and Rh NPs (metal = 0.037 mM) in water at room temperature and pressure with H_2 after 8 h of reaction.

Since we obtained, also in not very high amounts, the adipic acid, we tested its formation directly from *cis,cis*-hexenedioic acid, the isomer that can be derived also from the lignin and other biomass by biotechniques. In this case, surprisingly, the conversions and the yields were higher than with *trans,trans* isomer. In front of only a 30% of conversion (with 7% of adipic acid produced) in presence of Ru NPs, we converted 60% of the starting substrate and obtained 24% of adipic acid with Pt and 58% of conversion and 9% of adipic in presence of Pd NPs (Figures 5 and S29–S31). The use of an Rh NPs catalyst resulted in good performance: 80% of transformed muconic acid and 69% of adipic acid yield (Figures 5 and S32). The NMR spectra showed, during the course of reaction, the formation of 3-hexenedioic acid in variable amounts but not over 5% and the presence of isomer *cis,trans*-muconic acid ((2*Z*,4*E*)-hexa-2,4-dienedioic acid) that was the main product with Pt, Pd and Ru (Figures S33–S37). 2-Hexenedioic acid, carboxylated products and

trans,trans-muconic acid were never observed (Table S3). *Cis,trans*-muconic acid, the main product in our hydrogenation of *cis,cis*-substrate with Pt, Pd and Ru NPs, derived from an isomerization reaction, generally not reversible, can be triggered also by the heating and by the acid pH [23]. In fact, in acidic solutions (pH 2.5–4) the *cis,cis*-form isomerizes easily to *cis,trans*, also at room temperature, but above pH 4, it remains stable because of the intramolecular stabilization of the muconate form [23]. In our case, the reaction was carried out at pH 5 where muconic existed mainly as deprotonated species: we tested and verified its stability during 24 h in absence of M NPs at room temperature. So, our Ru, Pd and Pt NPs were revealed as active catalysts for the isomerization to *cis,trans*-muconate form but not effective for the hydrogenation to adipic acid.

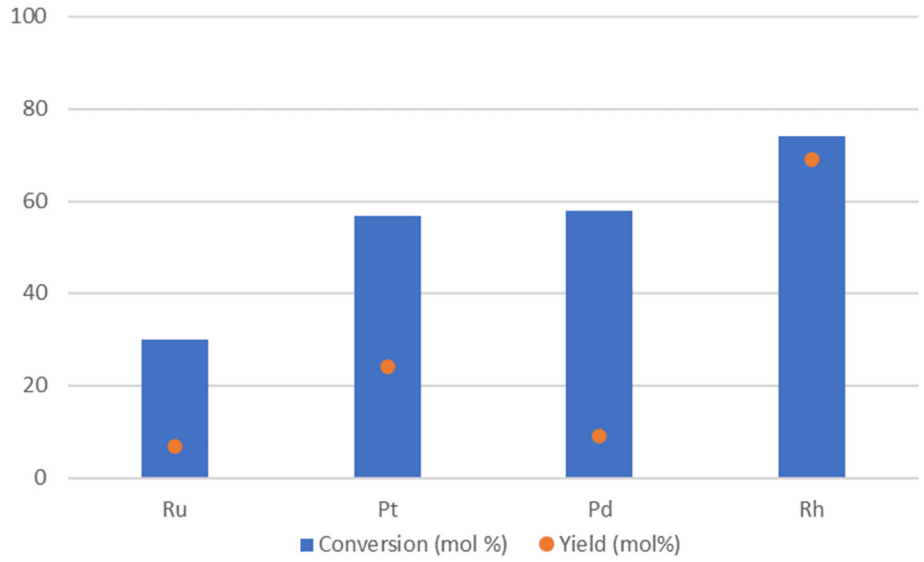

Figure 5. The conversion (mol%, blue) and yield (mol%, orange) of the hydrogenation reactions of *cis,cis*-muconic acid in presence of Ru, Pt, Pd and Rh NPs (metal = 0.037 mM) in water at room temperature and pressure with H_2 after 8 h of reaction.

In our reactions, 2-hexenedioic acid was observed only in the hydrogenation of the *trans,trans* isomer; it is well known that it is the first hydrogenated compound in the hydrogenation of muconic and muconate compounds, mostly at room temperature [30], and that it is transformed to 3-isomer [28]. In the presence of Pt NPs, 2-hexenedioic acid was the main product starting from *trans,trans*, suggesting the poor activity of these NPs as fully reduction catalyst for *trans,trans*-muconic acid. The potential steps of hexenedioic acid reductions in our conditions were resumed in the Scheme 3.

Comparing our M NPs in the hydrogenations of muconic acids, we can outline that Ru NPs were less active and also less selective (about 20% selectivity), the selectivity of Pt and Pd dropped down from *trans,trans*- to *cis,cis*-muconic acid (from 70% to 40 and 16% respectively). Rh NPs were proven to be very interesting catalyst for selective hydrogenation of dicarboxylic acids.

To test and to design the possibility of the recovery and the re-use of the metal catalyst, an additional experiment was carried out. When fumaric and maleic acids were completely transformed in presence of Rh NPs (about 4 h of reaction), an initial amount of the substrate was further added to the reaction mixture. In the following 4 h, the Rh NPs converted again 65% of the fumaric acid and 30% of the maleic acid to succinic acid without measurable amounts of by-products. We did not see drastic changes in the morphology of NPs, as it was reported in [46], but we can attribute this loss of reactivity to the polarity and the thickness variations in the layer of lignin that contributed to slow down the interaction between the organic compounds and the Rh cores.

3. Materials and Methods

3.1. Materials

Sodium lignosulphonate was a gift from Burgo Group S.p.A. (Tolmezzo, Italy). Potassium tetrachloroplatinate (K_2PtCl_4), and palladium chloride ($PdCl_2$) were purchased from Strem Chemicals Inc. (Bischheim, France) All the other reagents were bought from Merck KGaA (Darmstadt, Germany).

3.2. Synthesis and Characterization of M NPs

Lignin stabilized M NPs were prepared in accordance with our previous work [44]. Briefly, 0.010 g of $PdCl_2$ or 0.015 g of $RhCl_3 \cdot 3H_2O$ or 0.015 g of $RuCl_3 \cdot 3H_2O$ or 0.023 g of K_2PtCl_4 were added in 10 mL of water. Then 0.060 g of NaLig were introduced and the solution was stirred at 80 °C for about 2 h. The obtained NPs solution was used as such in the hydrogenation experiments.

The nanoparticles were fully characterized by TEM and XRD. The samples for the TEM analysis were prepared dropping 7 mL of the M NPs solution on a copper grid covered with an ultrathin carbon film and let it dry for at least 4 h. The TEM micrographs were collected by ZEISS Libra 200FE HRTEM, equipped with a second-generation W filter in column, that improves the contrast. The nanoparticle sizes were measured using iTEM TEM Imaging Platform Olympus and $d_m = \sum d_i n_i / \sum n_i$, where $\sum n_i$ is the number of particles [55]. More than 300 NPs were measured to estimate the sample mean size.

The samples for XRD analysis were prepared by solvent evaporation with a rotary evaporator at 40 °C of a 50 mL solution of M NPs and the resulting black solid powder was placed on the glass plate of the instrument. The XRD analysis was performed on a Miniflex II Rigaku automated power XRD system (Cu Kα radiation, 45 kV, 100 mA) (RINT 2500, Tokyo, Japan). Diffraction data were recorded using continuous scanning at 3° min^{-1}, with 0.010° steps and a PDF-4/mineral 2013 database.

The UV-vis analyses were carried out in 1 cm quartz cuvettes (Hellma) by properly diluting the NPs solution in ultrapure water. The UV-vis instrument was a Jenway 6505 spectrophotometer with a spectral window range of 200 nm to 800 nm.

NMR spectra were obtained using a Bruker Avance 300 spectrometer (7.05 Tesla) equipped with a high-resolution multinuclear probe that operated in the range of 30 MHz to 300 MHz. To eliminate the dominant water signal in the ^1H NMR spectra, water suppression was carried out using a presaturation sequence of a composite pulse (zgcppr Bruker sequence). A co-axial capillary tube that contained a 30 mM D_2O solution of 3-(trimethylsilyl) propionic-2,2,3,3-d_4 acid, sodium salt, was used as the reference.

3.3. Hydrogenation Reactions

0.0348 g of butenedioic acids (0.3 mmol) were introduced in a 20 mL vial with 15 mL of deionized water and then the solutions were sonicated for 5 minutes. In the case of muconic acids, 0.0426 g of acid (0.3 mmol) and 5 mL of NaOH 0.1 M (0.5 mmol) were added into 10 mL of deionized water and then the solutions were sonicated for 5 minutes. 100 mL of M NPs solution, corresponding to 0.56 μmol (0.037 mM) of the metal, were introduced in the vial. The mixture was vigorously fluxed with gaseous H_2 for 5 minutes. The reaction solution was then left under static H_2 atmosphere at room pressure (around 1 bar) and temperature (around 20 °C) and stirred for 8 h.

The reactions with the butenedioic acids were repeated in the same conditions but changing the amount of the added Rh NPs, as follows: 10 μL (0.0037 mM of the metal), 50 μL (0.0185 mM), 300 μL (0.111 mM), 500 μL (0.185 mM) of Rh NPs solution.

To verify the possibility of the re-use of the M NPS, after 4 h of the standard hydrogenation of the butenedioic acids in presence of Rh NPs, established the complete conversion of the substrate, 0.0348 g of butenedioic acids (0.3 mmol) were added to the reaction mixture. The solution was stirred for 4 additional hours.

The tests were performed in duplicate at minimum. The identity of each product was confirmed by comparison of ^{1}H NMR of pure compounds. The average reproducibility of quantitative measurements was within 5%.

4. Conclusions

The employed lignosulphonate proved to be effective as a reducing and stabilizing agent for the new Ru and Rh NPs which were fully characterized by TEM, XRD and UV-vis. All M NPs showed 100% of selectivity for succinic acid in the reduction of maleic and fumaric acid. The hydrogenations to succinic acid were principally used as models for the reactions of unsaturated dicarboxylic acids in water but we cannot fail to mention the future importance of succinic acid as an industrial platform to produce biopolymers.

Ru NPs were the less active catalysts in the hydrogenation reactions of maleic, fumaric and muconic acids; conversely, it is worthy of note that the activity of the Rh NPs was more constant than that of the other NPs: the selectivity in adipic acid was 100 % from *trans,trans*- and >85% from *cis,cis*-muconic acid while the adipic selectivity of the other catalysts was much lower and was dramatically observed in the case of Pd and Ru NPs. However, we should point out that all tested M NPs selectively catalyzed the reduction of C=C without evidence of potential decarboxylated or hydrated products.

These intriguing results open the way to explore the potential activity of Rh NPs, obtained with waste biomass, as catalysts in other (reduction) reactions carried out on the renewable compounds. Furthermore, this study, with additional essential research, could be a small step to the green production of nylon, starting from and valorizing the underutilized lignin.

Supplementary Materials: The following supporting information can be downloaded at: https://www.mdpi.com/article/10.3390/catal12101206/s1, Figure S1: TEM images of Pt NPs; Figure S2: UV-vis spectra of $RuCl_3$ and lignin in water solution (blue) and of Ru NPs (red). Inset: zoom on the 380–800 nm range; Figure S3: UV-vis spectra of $RhCl_3$ and lignin in water solution (blue) and of Rh NPs (red). Inset: zoom on the 380–800 nm range; Figure S4: XRD pattern of Rh NPs. Inset: XRD pattern of Rh performed by Match! software (version 3.10.2) including the crystallography open database (COD 2020); Figure S5: XRD pattern of Na Lig; Figure S6: XRD pattern of $RhCl_3$; Figure S7: XRD pattern of Ru NPs. Inset: XRD pattern of Ru performed by Match! software (version 3.10.2) including the crystallography open database (COD 2020); Figure S8: XRD pattern of $RuCl_3$; Figure S9: Time course of the hydrogenation of the maleic acid to succinic acid with Ru NPs (0.037 mM in Ru) in water at room temperature and pressure; Figure S10: Time course of the hydrogenation of the maleic acid to succinic acid with Pt NPs (0.037 mM in Pt) in water at room temperature and pressure; Figure S11: Time course of the hydrogenation of the maleic acid to succinic acid with Pd NPs (0.037 mM in Pd) in water at room temperature and pressure; Figure S12: Time course of the hydrogenation of the maleic acid to succinic acid with Rh NPs (0.037 mM in Rh) in water at room temperature and pressure; Figure S13: Time course of the hydrogenation of the fumaric acid to succinic acid with Ru NPs (0.037 mM in Ru) in water at room temperature and pressure; Figure S14: Time course of the hydrogenation of the fumaric acid to succinic acid with Pt NPs (0.037 mM in Pt) in water at room temperature and pressure; Figure S15: Time course of the hydrogenation of the fumaric acid to succinic acid with Pd NPs (0.037 mM in Pd) in water at room temperature and pressure; Figure S16: Time course of the hydrogenation of the fumaric acid to succinic acid with Rh NPs (0.037 mM in Rh) in water at room temperature and pressure; Figure S17: ^{1}H NMR spectrum of maleic acid 30 mM in water. The peak of 3-(trimethylsilyl) propionic-2,2,3,3-d_4 acid, sodium salt (at −0.2 ppm) was used as the reference; Figure S18: ^{1}H NMR spectrum of the reaction solution with maleic acid after 8 h in presence of Ru NPs in water. The peak of 3-(trimethylsilyl) propionic-2,2,3,3-d_4 acid, sodium salt (at −0.2 ppm) was used as the reference; Figure S19: ^{1}H NMR spectrum of the reaction solution with maleic acid after 4 h in presence of Rh NPs in water. The peak of 3-(trimethylsilyl) propionic-2,2,3,3-d_4 acid, sodium salt (at −0.2 ppm) was used as the reference; Figure S20: ^{1}H NMR spectrum of the reaction solution with maleic acid after 8 h in presence of Rh NPs in water. The peak of 3-(trimethylsilyl) propionic-2,2,3,3-d_4 acid, sodium salt (at −0.2 ppm) was used as the reference; Figure S21: ^{1}H NMR spectrum of fumaric acid 30 mM in water. The peak of 3-(trimethylsilyl) propionic-2,2,3,3-d_4 acid, sodium salt (at −0.2 ppm) was used as the reference; Figure S22: ^{1}H NMR spectrum of the reaction solution with maleic acid after 8 h in presence of Ru NPs in water.

The peak of 3-(trimethylsilyl) propionic-2,2,3,3-d_4 acid, sodium salt (at −0.2 ppm) was used as the reference; Figure S23: ^{1}H NMR spectrum of the reaction solution with maleic acid after 4 h in presence of Rh NPs in water. The peak of 3-(trimethylsilyl) propionic-2,2,3,3-d_4 acid, sodium salt (at −0.2 ppm) was used as the reference; Figure S24: ^{1}H NMR spectrum of the reaction solution with maleic acid after 8 h in presence of Rh NPs in water. The peak of 3-(trimethylsilyl) propionic-2,2,3,3-d_4 acid, sodium salt (at −0.2 ppm) was used as the reference; Figure S25: Time course of the hydrogenation of the *trans*,*trans*-muconic acid to adipic acid with Ru NPs (0.037 mM in Ru) in water at room temperature and pressure; Figure S26: Time course of the hydrogenation of the *trans*,*trans*-muconic acid to adipic acid with Pt NPs (0.037 mM in Pt) in water at room temperature and pressure; Figure S27: Time course of the hydrogenation of the *trans*,*trans*-muconic acid to adipic acid with Pd NPs (0.037 mM in Pd) in water at room temperature and pressure; Figure S28: Time course of the hydrogenation of the *trans*,*trans*-muconic acid to adipic acid with Rh NPs (0.037 mM in Rh) in water at room temperature and pressure; Figure S29: Time course of the hydrogenation of the *cis*,*cis*-muconic acid to adipic acid with Ru NPs (0.037 mM in Ru) in water at room temperature and pressure; Figure S30: Time course of the hydrogenation of the *cis*,*cis*-muconic acid to adipic acid with Pt NPs (0.037 mM in Pt) in water at room temperature and pressure; Figure S31: Time course of the hydrogenation of the *cis*,*cis*-muconic acid to adipic acid with Pd NPs (0.037 mM in Pd) in water at room temperature and pressure; Figure S32: Time course of the hydrogenation of the *cis*,*cis*-muconic acid to adipic acid with Rh NPs (0.037 mM in Rh) in water at room temperature and pressure; Figure S33: ^{1}H NMR spectrum of the *cis*,*cis*-muconic acid in water at pH 5. The peak of 3-(trimethylsilyl) propionic-2,2,3,3-d_4 acid, sodium salt (at −0.2 ppm) was used as the reference; Figure S34: ^{1}H NMR spectrum of the reaction solution with *cis*,*cis*-muconic acid after 8 h in presence of Ru NPs in water. The peak of 3-(trimethylsilyl) propionic-2,2,3,3-d_4 acid, sodium salt (at −0.2 ppm) was used as the reference; Figure S35: ^{1}H NMR spectrum of the reaction solution with *cis*,*cis*-muconic acid after 8 h in presence of Pt NPs in water. The peak of 3-(trimethylsilyl) propionic-2,2,3,3-d_4 acid, sodium salt (at −0.2 ppm) was used as the reference; Figure S36: ^{1}H NMR spectrum of the reaction solution with *cis*,*cis*-muconic acid after 8 h in presence of Pd NPs in water. The peak of 3-(trimethylsilyl) propionic-2,2,3,3-d_4 acid, sodium salt (at −0.2 ppm) was used as the reference; Figure S37: ^{1}H NMR spectrum of the reaction solution with *cis*,*cis*-muconic acid after 8 h in presence of Rh NPs in water. The peak of 3-(trimethylsilyl) propionic-2,2,3,3-d_4 acid, sodium salt (at −0.2 ppm) was used as the reference; Figure S38: ^{1}H NMR spectrum of *trans*,*trans*-muconic acid 30 mM in water at pH 5. The peak of 3-(trimethylsilyl) propionic-2,2,3,3-d_4 acid, sodium salt (at −0.2 ppm) was used as the reference; Figure S39: ^{1}H NMR spectrum of the reaction solution with *trans*,*trans*-muconic acid after 8 h in presence of Ru NPs in water. The peak of 3-(trimethylsilyl) propionic-2,2,3,3-d_4 acid, sodium salt (at −0.2 ppm) was used as the reference; Figure S40: ^{1}H NMR spectrum of the reaction solution with *trans*,*trans*-muconic acid after 8 h in presence of Pt NPs in water. The peak of 3-(trimethylsilyl) propionic-2,2,3,3-d_4 acid, sodium salt (at −0.2 ppm) was used as the reference; Figure S41: ^{1}H NMR spectrum of the reaction solution with *trans*,*trans*-muconic acid after 8 h in presence of Pd NPs in water. The peak of 3-(trimethylsilyl) propionic-2,2,3,3-d_4 acid, sodium salt (at −0.2 ppm) was used as the reference; Figure S42: ^{1}H NMR spectrum of the reaction solution with *trans*,*trans*-muconic acid after 8 h in presence of Rh NPs in water. The peak of 3-(trimethylsilyl) propionic-2,2,3,3-d_4 acid, sodium salt (at −0.2 ppm) was used as the reference; Table S1: Yield of succinic acid and conversion of maleic and fumaric acids with Rh NPs at different concentrations after 4 h of reaction in water at room temperature and pressure with H_2; Table S2: Yield of products and conversion of *trans*,*trans*-muconic acid with M NPs after 8 h of reaction in water at room temperature and pressure with H_2; Table S3: Yield of products and conversion of *cis*,*cis*-muconic acid with M NPs after 8 h of reaction in water at room temperature and pressure with H_2.

Author Contributions: Conceptualization, L.T. and N.d.; methodology, L.T. and F.C.; formal analysis, A.M. and A.M.F.; investigation, A.M. and A.M.F.; resources, N.d. and A.M.F.; writing—original draft preparation, L.T. and A.M.; writing—review and editing, N.d. and F.C.; funding acquisition, N.d. and L.T. All authors have read and agreed to the published version of the manuscript.

Funding: This research was funded by Consorzio per l'Innovazione Tecnologica-Qualità e Sicurezza degli Alimenti (ITQSA), project no. DM 69961318.

Data Availability Statement: Not applicable.

Conflicts of Interest: The authors declare no conflict of interest. The funders had no role in the design of the study; in the collection, analyses, or interpretation of data; in the writing of the manuscript; or in the decision to publish the results.

References

1. Grand View Research. *Nylon Market Size, Share & Trends Analysis Report By Product (Nylon 6, Nylon 66), By Application (Automobile, Electrical & Electronics, Engineering Plastics, Textiles), By Region, And Segment Forecasts, Grand View Research, San Francisco, US.* Vol. GVR-1-6803. *2022–2030*; 2022.
2. Tullo, A. Industry braces for nylon 6,6 shortage. *CEN Glob. Enterp.* **2018**, *96*, 22–23. https://doi.org/10.1021/cen-09640-feature3.
3. European Bioplastics. *Market Update 2020: Bioplastics Continue to Become Mainstream as the Global Bioplastics Market Is Set to Grow by 36 Percent over the next 5 Years*; European Bioplastics, Berlin, Germany. 2020
4. Van de Vyver, S.; Román-Leshkov, Y. Emerging catalytic processes for the production of adipic acid. *Catal. Sci. Technol.* **2013**, *3*, 1465–1479. https://doi.org/10.1039/c3cy20728e.
5. Reimer, R.A.; Slaten, C.S.; Seapan, M.; Koch, T.A.; Triner, V.G. Adipic Acid Industry—N_2O Abatement. In *Non-CO_2 Greenhouse Gases: Scientific Understanding, Control and Implementation*; Springer: Dordrecht, The Netherlands, 2000; pp. 347–358.
6. Portmann, R.W.; Daniel, J.S.; Ravishankara, A.R. Stratospheric ozone depletion due to nitrous oxide: Influences of other gases. *Philos. Trans. R. Soc. B: Biol. Sci.* **2012**, *367*, 1256–1264. https://doi.org/10.1098/rstb.2011.0377.
7. Donen, S.; Hash, K.; Smith, T.; Jensen, K. Nitric Acid Oxidation Processes. U.S. Patent 9,187,398, filed 12 March 2014.
8. Zimmerman, J.B.; Anastas, P.T.; Erythropel, H.C.; Leitner, W. Designing for a green chemistry future. *Science* **2020**, *367*, 397–400. https://doi.org/10.1126/science.aay3060.
9. Capece, N.; Sadier, A.; Ferraz, C.P.; Thuriot-Roukos, J.; Pietrowski, M.; Zieliński, M.; Paul, S.; Cavani, F.; Wojcieszak, R. Aerobic oxidation of 1,6-hexanediol to adipic acid over Au-based catalysts: The role of basic supports. *Catal. Sci. Technol.* **2020**, *10*, 2644–2651. https://doi.org/10.1039/d0cy00183j.
10. D'Alessandro, N.; Liberatore, L.; Tonucci, L.; Morvillo, A.; Bressan, M. Direct synthesis of adipic acid by mono-persulfate oxidation of cyclohexane, cyclohexanone or cyclohexanol catalyzed by water-soluble transition-metal complexes. *New J. Chem.* **2001**, *25*, 1319–1324. https://doi.org/10.1039/b102499j.
11. Mazzi, A.; Paul, S.; Cavani, F.; Wojcieszak, R. Cyclohexane Oxidation to Adipic Acid Under Green Conditions: A Scalable and Sustainable Process. *ChemCatChem* **2018**, *10*, 3680–3682. https://doi.org/10.1002/cctc.201800419.
12. Yan, W.; Zhang, G.; Wang, J.; Liu, M.; Sun, Y.; Zhou, Z.; Zhang, W.; Zhang, S.; Xu, X.; Shen, J.; et al. Recent Progress in Adipic Acid Synthesis Over Heterogeneous Catalysts. *Front. Chem.* **2020**, *8*, 1–12. https://doi.org/10.3389/fchem.2020.00185.
13. Lesage, G.; Peñate, I.Q.; Franceschi, S.; Perez, E.; Garrigues, J.-C.; Poux, M.; Cognet, P. Sustainable process for adipic acid production from cyclohexene in microemulsion. *Catal. Today* **2020**, *346*, 40–45. https://doi.org/10.1016/j.cattod.2019.02.065.
14. Braga, M.; Ferreira, P.M.; Almeida, J.R.M. Screening method to prioritize relevant bio-based acids and their biochemical processes using recent patent information. *Biofuels Bioprod. Biorefining* **2021**, *15*, 231–249. https://doi.org/10.1002/bbb.2156.
15. Polen, T.; Spelberg, M.; Bott, M. Toward biotechnological production of adipic acid and precursors from biorenewables. *J. Biotechnol.* **2013**, *167*, 75–84. https://doi.org/10.1016/j.jbiotec.2012.07.008.
16. van Duuren, J.B.J.H.; Wijte, D.; Karge, B.; dos Santos, V.A.M.; Yang, Y.; Mars, A.E.; Eggink, G. pH-stat fed-batch process to enhance the production of cis, cis-muconate from benzoate by Pseudomonas putida KT2440-JD1. *Biotechnol. Prog.* **2012**, *28*, 85–92. https://doi.org/10.1002/btpr.709.
17. Draths, K.M.; Frost, J.W. Environmentally compatible synthesis of adipic acid from D-glucose. *J. Am. Chem. Soc.* **1994**, *116*, 399–400. https://doi.org/10.1021/ja00080a057.
18. Becker, J.; Lange, A.; Fabarius, J.; Wittmann, C. Top value platform chemicals: Bio-based production of organic acids. *Curr. Opin. Biotechnol.* **2015**, *36*, 168–175. https://doi.org/10.1016/j.copbio.2015.08.022.
19. Sonoki, T.; Takahashi, K.; Sugita, H.; Hatamura, M.; Azuma, Y.; Sato, T.; Suzuki, S.; Kamimura, N.; Masai, E. Glucose-Free *cis*,*cis*-Muconic Acid Production via New Metabolic Designs Corresponding to the Heterogeneity of Lignin. *ACS Sustain. Chem. Eng.* **2018**, *6*, 1256–1264. https://doi.org/10.1021/acssuschemeng.7b03597.
20. Vardon, D.R.; Franden, M.A.; Johnson, C.W.; Karp, E.M.; Guarnieri, M.T.; Linger, J.G.; Salm, M.J.; Strathmann, T.J.; Beckham, G.T. Adipic acid production from lignin. *Energy Environ. Sci.* **2015**, *8*, 617–628. https://doi.org/10.1039/c4ee03230f.
21. Johnson, C.W.; Abraham, P.E.; Linger, J.G.; Khanna, P.; Hettich, R.L.; Beckham, G.T. Eliminating a global regulator of carbon catabolite repression enhances the conversion of aromatic lignin monomers to muconate in Pseudomonas putida KT2440. *Metab. Eng. Commun.* **2017**, *5*, 19–25. https://doi.org/10.1016/j.meteno.2017.05.002.
22. Renewable adipic acid from the hydrogenation of trans, trans-muconic acid: Selection of a three phases kinetic model. *Chem. Eng. Trans.* **2017**, *57*, 931–936. https://doi.org/10.3303/CET1757156.
23. Carraher, J.M.; Pfennig, T.; Rao, R.G.; Shanks, B.H.; Tessonnier, J.-P. cis,cis-Muconic acid isomerization and catalytic conversion to biobased cyclic-C_6-1,4-diacid monomers. *Green Chem.* **2017**, *19*, 3042–3050. https://doi.org/10.1039/c7gc00658f.
24. Carraher, J.M.; Carter, P.; Rao, R.G.; Forrester, M.J.; Pfennig, T.; Shanks, B.H.; Cochran, E.W.; Tessonnier, J.-P. Solvent-driven isomerization of *cis*,*cis*-muconic acid for the production of specialty and performance-advantaged cyclic biobased monomers. *Green Chem.* **2020**, *22*, 6444–6454. https://doi.org/10.1039/d0gc02108c.
25. Matthiesen, J.E.; Carraher, J.M.; Vasiliu, M.; Dixon, D.A.; Tessonnier, J.-P. Electrochemical Conversion of Muconic Acid to Biobased Diacid Monomers. *ACS Sustain. Chem. Eng.* **2016**, *4*, 3575–3585. https://doi.org/10.1021/acssuschemeng.6b00679.
26. She, X.; Brown, H.M.; Zhang, X.; Ahring, B.K.; Wang, Y. Selective Hydrogenation of Trans,Trans-Muconic Acid to Adipic Acid over a Titania-Supported Rhenium Catalyst. *ChemSusChem* **2011**, *4*, 1071–1073. https://doi.org/10.1002/cssc.201100020.
27. Zhang, H.; Li, X.; Su, X.; Ang, E.L.; Zhang, Y.; Zhao, H. Production of Adipic Acid from Sugar Beet Residue by Combined Biological and Chemical Catalysis. *ChemCatChem* **2016**, *8*, 1500–1506. https://doi.org/10.1002/cctc.201600069.

28. Capelli, S.; Motta, D.; Evangelisti, C.; Dimitratos, N.; Prati, L.; Pirola, C.; Villa, A. Bio Adipic Acid Production from Sodium Muconate and Muconic Acid: A Comparison of two Systems. *ChemCatChem* **2019**, *11*, 3075–3084. https://doi.org/10.1002/cctc.201900343.
29. Capelli, S.; Motta, D.; Evangelisti, C.; Dimitratos, N.; Prati, L.; Pirola, C.; Villa, A. Effect of Carbon Support, Capping Agent Amount, and Pd NPs Size for Bio-Adipic Acid Production from Muconic Acid and Sodium Muconate. *Nanomaterials* **2020**, *10*, 505. https://doi.org/10.3390/nano10030505.
30. Vardon, D.R.; Rorrer, N.A.; Salvachúa, D.; Settle, A.E.; Johnson, C.W.; Menart, M.J.; Cleveland, N.S.; Ciesielski, P.N.; Steirer, K.X.; Dorgan, J.R.; et al. cis,cis-Muconic acid: Separation and catalysis to bio-adipic acid for nylon-6,6 polymerization. *Green Chem.* **2016**, *18*, 3397–3413. https://doi.org/10.1039/c5gc02844b.
31. Scelfo, S.; Pirone, R.; Russo, N. Highly efficient catalysts for the synthesis of adipic acid from cis,cis-muconic acid. *Catal. Commun.* **2016**, *84*, 98–102. https://doi.org/10.1016/j.catcom.2016.06.013.
32. Hočevar, B.; Prašnikar, A.; Huš, M.; Grilc, M.; Likozar, B. H_2 -Free Re-Based Catalytic Dehydroxylation of Aldaric Acid to Muconic and Adipic Acid Esters. *Angew. Chem. Int. Ed.* **2021**, *60*, 1244–1253. https://doi.org/10.1002/anie.202010035.
33. Bozell, J.J.; Petersen, G.R. Technology development for the production of biobased products from biorefinery carbohydrates—The US Department of Energy's "Top 10" revisited. *Green Chem.* **2010**, *12*, 539–554. https://doi.org/10.1039/b922014c.
34. Tonucci, L.; Coccia, F.; Bressan, M.; D'Alessandro, N. Mild Photocatalysed and Catalysed Green Oxidation of Lignin: A Useful Pathway to Low-Molecular-Weight Derivatives. *Waste Biomass Valorization* **2011**, *3*, 165–174. https://doi.org/10.1007/s12649-011-9102-6.
35. Dros, A.B.; Larue, O.; Reimond, A.; De Campo, F.; Pera-Titus, M. Hexamethylenediamine (HMDA) from fossil- vs. bio-based routes: An economic and life cycle assessment comparative study. *Green Chem.* **2015**, *17*, 4760–4772. https://doi.org/10.1039/C5GC01549A.
36. Nandiwale, K.Y.; Danby, A.M.; Ramanathan, A.; Chaudhari, R.V.; Motagamwala, A.H.; Dumesic, J.A.; Subramaniam, B. Enhanced Acid-Catalyzed Lignin Depolymerization in a Continuous Reactor with Stable Activity. *ACS Sustain. Chem. Eng.* **2020**, *8*, 4096–4106. https://doi.org/10.1021/acssuschemeng.9b06556.
37. Li, S.; Li, Z.-J.; Yu, H.; Sytu, M.R.; Wang, Y.; Beeri, D.; Zheng, W.; Sherman, B.D.; Yoo, C.G.; Leem, G. Solar-Driven Lignin Oxidation via Hydrogen Atom Transfer with a Dye-Sensitized TiO_2 Photoanode. *ACS Energy Lett.* **2019**, *5*, 777–784. https://doi.org/10.1021/acsenergylett.9b02391.
38. Sun, Z.; Barta, K. Cleave and couple: Toward fully sustainable catalytic conversion of lignocellulose to value added building blocks and fuels. *Chem. Commun.* **2018**, *54*, 7725–7745. https://doi.org/10.1039/c8cc02937g.
39. Den, W.; Sharma, V.K.; Lee, M.; Nadadur, G.; Varma, R.S. Lignocellulosic Biomass Transformations via Greener Oxidative Pretreatment Processes: Access to Energy and Value-Added Chemicals. *Front. Chem.* **2018**, *6*, 141. https://doi.org/10.3389/fchem.2018.00141.
40. Wang, S.; Ma, S.; Xu, C.; Liu, Y.; Dai, J.; Wang, Z.; Liu, X.; Chen, J.; Shen, X.; Wei, J.; et al. Vanillin-Derived High-Performance Flame Retardant Epoxy Resins: Facile Synthesis and Properties. *Macromolecules* **2017**, *50*, 1892–1901. https://doi.org/10.1021/acs.macromol.7b00097.
41. Llevot, A.; Grau, E.; Carlotti, S.; Grelier, S.; Cramail, H. From Lignin-derived Aromatic Compounds to Novel Biobased Polymers. *Macromol. Rapid Commun.* **2016**, *37*, 9–28. https://doi.org/10.1002/marc.201500474.
42. Cao, Z.; Dierks, M.; Clough, M.T.; de Castro, I.B.D.; Rinaldi, R. A Convergent Approach for a Deep Converting Lignin-First Biorefinery Rendering High-Energy-Density Drop-in Fuels. *Joule* **2018**, *2*, 1118–1133. https://doi.org/10.1016/j.joule.2018.03.012.
43. Wang, H.; Yang, B.; Zhang, Q.; Zhu, W. Catalytic routes for the conversion of lignocellulosic biomass to aviation fuel range hydrocarbons. *Renew. Sustain. Energy Rev.* **2020**, *120*, 109612. https://doi.org/10.1016/j.rser.2019.109612.
44. Coccia, F.; Tonucci, L.; Bosco, D.; Bressan, M.; D'Alessandro, N. One-pot synthesis of lignin-stabilised platinum and palladium nanoparticles and their catalytic behaviour in oxidation and reduction reactions. *Green Chem.* **2012**, *14*, 1073–1078. https://doi.org/10.1039/c2gc16524d.
45. Coccia, F.; Tonucci, L.; D'Alessandro, N.; D'Ambrosio, P.; Bressan, M. Palladium nanoparticles, stabilized by lignin, as catalyst for cross-coupling reactions in water. *Inorg. Chim. Acta* **2013**, *399*, 12–18. https://doi.org/10.1016/j.ica.2012.12.035.
46. Di Pietrantonio, K.; Coccia, F.; Tonucci, L.; D'Alessandro, N.; Bressan, M. Hydrogenation of allyl alcohols catalyzed by aqueous palladium and platinum nanoparticles. *RSC Adv.* **2015**, *5*, 68493–68499. https://doi.org/10.1039/C5RA13840J.
47. Coccia, F.; Tonucci, L.; Del Boccio, P.; Caporali, S.; Hollmann, F.; D'Alessandro, N. Stereoselective Double Reduction of 3-Methyl-2-cyclohexenone, by Use of Palladium and Platinum Nanoparticles, in Tandem with Alcohol Dehydrogenase. *Nanomaterials* **2018**, *8*, 853. https://doi.org/10.3390/nano8100853.
48. Gherib, H.; Boudjahem, A.G.; Medjahdi, G. Effect of Preparation Method and Support on Catalytic Behavior of Rhodium Nanoparticles in Styrene Hydrogenation. *Kinet. Catal.* **2020**, *61*, 466–472. https://doi.org/10.1134/s0023158420030106.
49. Akbayrak, S. Rhodium(0) nanoparticles supported on ceria as catalysts in hydrogenation of neat benzene at room temperature. *J. Colloid Interface Sci.* **2018**, *530*, 459–464. https://doi.org/10.1016/j.jcis.2018.07.011.
50. Wang, W.; Ciganda, R.; Wang, C.; Escobar, A.; Martinez-Villacorta, A.M.; Ramírez, M.D.L.; Hernández, R.; Moya, S.E.; Ruiz, J.; Hamon, J.-R.; et al. High catalytic activity of Rh nanoparticles generated from cobaltocene and $RhCl_3$ in aqueous solution. *Inorg. Chem. Front.* **2019**, *6*, 2704–2708. https://doi.org/10.1039/c9qi00742c.

51. Moos, G.; Emondts, M.; Bordet, A.; Leitner, W. Selective Hydrogenation and Hydrodeoxygenation of Aromatic Ketones to Cyclohexane Derivatives Using a Rh@SILP Catalyst. *Angew. Chem. Int. Ed.* **2020**, *59*, 11977–11983. https://doi.org/10.1002/anie.201916385.
52. Hamdy, M.S.; Alhanash, A.M.; Benaissa, M.; Alsalme, A.; Alharthi, F.A.; Al-Zaqri, N. Rhodium Nanoparticles Incorporated Mesoporous Silica as an Active Catalyst for Cyclohexene Hydrogenation under Ambient Conditions. *Catalysts* **2020**, *10*, 925. https://doi.org/10.3390/catal10080925.
53. Morfin, F.; Blondeau, L.; Provost, K.; Malouche, A.; Piccolo, L.; Zlotea, C. Absorbed hydrogen enhances the catalytic hydrogenation activity of Rh-based nanocatalysts. *Catal. Sci. Technol.* **2018**, *8*, 2707–2715. https://doi.org/10.1039/c8cy00522b.
54. Crespo, I.; Dominguez, O.; Baricelli, P.; Borusiak, M.; Omaña, O.; Castro, W.; Rosales, M. Biphasic hydrogenation of eugenol with ruthenium and rhodium nanoparticles stabilized in ionic liquids. *J. Chil. Chem. Soc.* **2020**, *65*, 4982–4987. https://doi.org/10.4067/s0717-97072020000404982.
55. Borodziński, A.; Bonarowska, M. Relation between Crystallite Size and Dispersion on Supported Metal Catalysts. *Langmuir* **1997**, *13*, 5613–5620. https://doi.org/10.1021/la962103u.
56. Creighton, J.A.; Eadon, D.G. Ultraviolet–visible absorption spectra of the colloidal metallic elements. *J. Chem. Soc. Faraday Trans.* **1991**, *87*, 3881–3891. https://doi.org/10.1039/ft9918703881.
57. Papp, S.; Patakfalvi, R.; Dékány, I. Formation and Stabilization of Noble Metal Nanoparticles. *Croat. Chem. Acta* **2007**, *80*, 493–502.
58. Zhang, H.; Xia, X.; Li, W.; Zeng, J.; Dai, Y.; Yang, D.; Xia, Y. Facile Synthesis of Five-fold Twinned, Starfish-like Rhodium Nanocrystals by Eliminating Oxidative Etching with a Chloride-Free Precursor. *Angew. Chem. Int. Ed.* **2010**, *49*, 5296–5300. https://doi.org/10.1002/anie.201002546.
59. Gopiraman, M.; Saravanamoorthy, S.; Ullah, S.; Ilangovan, A.; Kim, I.S.; Chung, I.M. Reducing-agent-free facile preparation of Rh-nanoparticles uniformly anchored on onion-like fullerene for catalytic applications. *RSC Adv.* **2020**, *10*, 2545–2559. https://doi.org/10.1039/c9ra09244g.
60. Gopiraman, M.; Karvembu, R.; Kim, I.S. Highly Active, Selective, and Reusable RuO_2/SWCNT Catalyst for Heck Olefination of Aryl Halides. *ACS Catal.* **2014**, *4*, 2118–2129. https://doi.org/10.1021/cs500460m.